Lab on a Chip

Sorting by Interfacial Tension (SIFT): Label-Free Selection of Live Cells Based on Single-Cell Metabolism

Journal:	*Lab on a Chip*
Manuscript ID	LC-ART-12-2018-001328.R1
Article Type:	Paper
Date Submitted by the Author:	26-Feb-2019
Complete List of Authors:	Pan, Ching; Santa Clara University, Chemistry and Biochemistry Horvath, Daniel; Santa Clara University, Chemistry and Biochemistry Braza, Samuel; Santa Clara University, Chemistry and Biochemistry Moore, Trevor; Santa Clara University, Chemistry and Biochemistry Lynch, Annabella; Santa Clara University, Chemistry and Biochemistry Feit, Cameron; Santa Clara University, Chemistry and Biochemistry Abbyad, Paul; Santa Clara University, Chemistry and Biochemistry

SCHOLARONE™
Manuscripts

Sorting by Interfacial Tension (SIFT): Label-Free Selection of Live Cells Based on Single-Cell Metabolism

Ching W. Pan#, Daniel G. Horvath#, Samuel Braza, Trevor Moore, Annabella Lynch, Cameron Feit, Paul Abbyad

# Both authors contributed equally to this work

Department of Chemistry and Biochemistry, Santa Clara University, Santa Clara, CA, 95053, USA

* corresponding author: pabbyad@scu.edu

ABSTRACT

Selection of live cells from a population is critical in many biological studies and biotechnologies. We present here a novel droplet microfluidic approach that allows for label-free and passive selection of live cells using the glycolytic activity of individual cells. It was observed that with the use of a specific surfactant utilized to stabilize droplet formation, the interfacial tension of droplets was very sensitive to pH. After incubation, cellular lactate release results in droplets containing a live cell to attain a lower pH than other droplets. This enables the sorting of droplets containing live cells when confined droplets flow over a microfabricated trench oriented diagonally with respect to the direction of flow. The technique is demonstrated with human U87 glioblastoma cells for the selection of only droplets containing a live cell while excluding either empty droplets or droplets containing a dead cell. This label-free sorting method, dubbed Sorting by Interfacial Tension (SIFT) presents a new strategy to sort diverse cell types based on metabolic activity.

Introduction

The selection of cells is of general interest across cell biology, medicine, and biotechnology. An important utilization of cell selection is to remove nonviable mammalian cells from cellular suspension, a function critical in several clinical applications including monoclonal antibody production, improving clinical outcomes of cell therapies and improving accuracy of biomedical assays and drug screening.[1,2] The workhorse of cell sorting is fluorescent-activated cell sorting (FACS), which provides high throughput and high selectivity of live cells. Alternatively, encapsulating cells in microfluidic droplets expands functionality by enabling selection based on cell excretions.[3,4] Droplet sorters primarily use electric fields to select droplets over a defined signal threshold,[3,5] with recently reported sorting rates of 30 kHz.[6] Although powerful, these techniques are expensive; they require the observation of the cell or droplet (usually by fluorescence) and synchronization with an active component for selection or sorting. Magnetic-activated cell sorting (MACS) uses magnetic particles bound to surface markers for sorting, but remains costly, results in high cell loss, and requires specific labels on membranes of cells of interest for selection.[7]

Many label-free microfluidic techniques have thus been developed to isolate live cells using physical attributes including size, density, stiffness and electrical polarizability. These include acoustophoresis where acoustic pressure waves move larger live cells to a selection channel, removing dead cells that has shrunk as part of the apoptotic mechanism.[8,9] Similarly, inertial microfluidics uses differences in size and deformability between live and dead cells to sort and separate the two populations.[10,11] The movement of cells when travelling through an array of posts, deterministic lateral

displacement, can also separate live cells based on size, shape and deformability.[12] Dielectric properties of cells can also be leveraged for live sorting by techniques such as dielectrophoresis.[13,14] These techniques are cost effective and offer good throughput. However, as current label-free techniques rely solely on physical attributes, they can lack selectivity.[15] In addition, physical changes, such as morphology changes, may take hours to manifest[16]. These techniques do not sort directly based on cell function or activity. Glycolytic activity is an indicator of viability across varied cell types [17,18] and altered glycolysis is of critical importance to many disease states, most notably cancer.[19,20]

The glycolysis metabolic pathway leads to the cellular excretion of lactate and is typically the primary source of acidification of the extracellular environment.[21] This acidification of the surrounding media is detected by commercial instruments that measure glycolytic activity of cell populations (e.g., Seahorse XF24 Extracellular Flux Analyzer electrode system[22]). As observed close to a century ago by Otto Warburg, cancer cells, in particular, display high rates of lactate release even in the presence of oxygen.[23,24] A recent communication[25] presented a new way to detect, but not isolate, single cancer cells by encapsulating the cells in picoliter droplets and measuring the change of pH due to lactate secretion. Droplet acidification is quick, with a noticeable change in droplet pH occurring in less than 2 minutes. Target cancer cells display a decrease of 0.5 pH units or more within 10 minutes.

The physical properties of aqueous droplets in oil have been used previously for analyte detection or sorting. For example, the lab of Amar Basu used changes in surface tension to sort droplets with and without bovine serine albumin based on migration in a

surfactant gradient.[26,27] We present here a method to sort and isolate live cells using changes in interfacial tension based on single-cell lactate secretion.

The passive sorting mechanism utilizes a change in droplet interfacial tension resulting from pH differences to control droplet flow position. We dubbed this strategy of droplet sorting: *Sorting based on Interfacial Tension* or SIFT. We demonstrate the use of the technique to sort droplets of different pH. Single cell occupancy is often a prerequisite for many single-cell analysis techniques in droplets.[28] The technique is used to select single-cell encapsulated droplets containing U87 human glioblastoma cells from empty droplets. To our knowledge, this is the first passive technique that uses cellular metabolism to ensure single-cell occupancy in droplets. SIFT is also applied to sort live vs dead cells in a population. The technique enables the simple and accurate selection of droplets containing live cells while removing the need for a label or costly active droplet sorting technology. It presents a general and simple strategy to sort cells based on single-cell metabolism.

Materials and Methods

Pendant Drop: Interfacial tension measurements were performed on FTA 1000 (First Ten Angstroms) goniometer. Aqueous droplets in oil were produced using a 20 gauge j-needle. Droplets were allowed to equilibrate for 10-20 minutes prior to measurement. QX100 Droplet Generation Oil (Biorad) was diluted with perfluorinated oil, NOVEC 7500 (3M) for measurement. Aqueous droplets in undiluted QX100 Droplet Generation Oil had very low interfacial tension and detached within seconds from the needle, resulting in inconsistent measurements. Interfacial tension was determined by fits to the droplet shape using First Ten Angstroms analysis software.

Cells: U87 human glioblastoma cancer cells (gift from B. Lu, Santa Clara University) were grown at 37 °C and 5% CO_2 in Dulbecco Modified Eagle Medium (DMEM) supplemented with 10% fetal bovine serum, 1% penicillin-streptomycin. U87 cells were trypsinized and counted before being used. Cells were rinsed three times with 1x PBS and incubated with the a viability fluorescent dye, Calcein AM (Thermofischer), for 1 hour in a 37 °C and 4% CO_2 incubator. Immediately prior to experiments, cells were spun down and resuspended in a 1:1 mixture of 2.5mM PBS buffer and DMEM media without fetal bovine serum (deproteinated media) or sodium bicarbonate. Also present in the final cellular solutions was pluronic F-68 (1% w/w) and optiprep (15% v/v). The addition of pluronic served to increase cell viability while the optiprep limited cell sedimentation in the tubing and droplets during the experiment. In some experiments, pyranine (AAT Bioquest) was added to the cell solution at a concentration of 1.9 mM as a fluorescent ratiometric pH probe. Both the pH and the osmolality (using a Vapro Vapor Pressure Osmometer 5520, Wescor) of solutions were verified prior to use. In live vs. dead cell assay, half the cells were treated as stated above and the other half incubated in 4% paraformaldehyde solution for 1 hour at ambient conditions, rendering the cells nonviable. The nonviable cells were rinsed two times with PBS before incubating with the viability fluorescent dye. After incubation, live and dead cells were spun into pellets and resuspended in a 1:1 mixture of 2.5mM PBS buffer and DMEM media and cells mixed together at about an equal ratio of live to dead cells before injection on chip.

Microfluidic Device: Polydimethylsiloxane (PDMS) microfluidic chips with channel depth modulations were fabricated using the dry-film photoresist soft lithography technique described by Stephan *et al.*[29]. The technique enabled rapid prototyping of

multi-level structures. The PDMS chips were then plasma-bonded to a glass slide. To render the internal channel surface hydrophobic, Novec™ 1720 Electronic Grade Coating (3M) was flowed into the microchannel and the chip was heated for 30 minutes at 150 °C. The surface treatment prevented wetting and contact of the aqueous droplets with the channel walls.

Measurements: The temperature of the chip was maintained at 37°C using a microscope heating stage with control module with temperature feedback (CHS-1 heating plate with TC-324C temperature controller, Warner Instruments). Fluid flow was controlled using computer-controlled syringe pumps (Nemesys, Cetoni). Images were taken with a 4X objective on an inverted fluorescence microscopes (Olympus IX-50) equipped with shuttered LED fluorescence excitation source (Spectra-X light engine, Lumencor) and CMOS camera (Orca Flash 2.8 Hamamatsu). The excitation source allowed for alternate violet (395nm BP 25nm) and blue excitation (440 nm BP 20nm) for ratiometric pH determination. Images were also acquired on an inverted fluorescence microscope (IX-51) equipped with a shuttered LED fluorescence excitation source (SOLA-SE-II, Lumencor) and a high speed camera (VEO-410, Vision Research). Images and videos were analyzed using ImageJ.[30]

Results and Discussion

In droplet microfluidics,[31] biological and chemical reagents are encapsulated in aqueous droplets transported in inert oil enabling increases in throughput in directed evolution,[4] digital PCR,[32] drug screening[33] and large-scale biological assays.[4,33–35] Perfluorinated oils, due to their good biocompatibility, are often used as external oil to generate and transport aqueous droplets. Surfactants, typically polymers consisting of

both a hydrophilic and perfluorinated moieties, are dispersed in the oil phase. Surfactants reduce droplet interfacial tension (surface tension between the aqueous droplet and oil) and thus aid in the formation of droplets and inhibit droplet coalescence, while reducing wetting of droplets on channel walls. In rare cases, surfactants have played additional roles as fluorescent probes of the droplet interface or as catalysts for chemical reactions.[36,37]

QX100 Droplet Generation Oil for Probes (Biorad), hereby called QX100, is a product designed for use with the QX100/QX200 digital droplet PCR system. QX100 enables the production of stable droplets and contains a surfactant dissolved in perfluorinated oil. It was observed that for aqueous droplets in QX100 oil, the interfacial tension of droplets was dependent on droplet pH. Between a pH range relevant for biological samples (6.0-8.0), a decrease in pH led to a large increase in interfacial tension as measured by pendant droplet (Fig. 1a).

It should be noted that in the pendant droplet measurements presented, the QX100 was diluted 100 fold by mass with the perfluorinated solvent, Novec 7500. On chip experiments used undiluted QX100. Droplets in undiluted QX100 had very low interfacial tension rendering measurements by pendant drop inconsistent. Therefore the values of interfacial tension presented in Figure 1a would be higher than conditions used on chip. However, the sensitivity of interfacial tension with pH is maintained in undiluted QX100 as higher pH droplets showed a marked increase in deformability on chip.

A change in interfacial tension with pH for droplets in QX100 was observed in all biological relevant solutions studied including: PBS buffer, PBS buffer with added glucose, DMEM media, and DMEM in the presence of additives (such as pluronic F-68

and optiprep). The change in interfacial tension is observed both at room temperature (Fig 1a) and 37° C (Fig. S1).

The sensitivity of interfacial tension with pH is unique to QX100. The interfacial tension dependence was not observed for Novec 7500 perfluorinated oil without surfactant (Fig. S2a). It was also not observed for commonly used perfluorinated surfactants dissolved in Novec 7500 such as 008 fluorosurfactant (Ran Technologies), Picosurf I and II (Dolomite Microfluidics) (Fig. S2b-d). Proprietary surfactant structure hinders the investigation of the mechanism of change in interfacial tension for QX100, but preliminary hypothesis suggests that the change may be due to an altered fluorosurfactant protonation state. We show here that this change in droplet interfacial tension based on pH can be applied to droplet selection.

DEVICE

The full channel geometry is shown in Figure 1b with the general flow of droplets in the device from left to right. Inlets and outlets of the chip are labelled in the figure for reference in the sections below. Typical flow rates used in experiments are summarized in Table S1. The function of device has three major sequential steps: cell encapsulation in droplets, cell incubation to allow for changes in pH due to lactate release and finally, droplet sorting using differences in interfacial tension.

Two Aqueous Inlets are used for injecting cellular solutions. These dual inlets allow for the addition of reagents to the cellular solution just prior to droplet formation. However, in the use described in this paper only one of the Aqueous Inlets was utilized. Droplets are formed at a flow focuser[19] using the oil 0.1% w/w picosurf-1 (Dolomite) in Novec 7500 provided from the Oil Inlet. A negative flow is maintained at the Oil Outlet,

to remove oil but not droplets from the device.[38] This allows for tight packet of droplets in the droplet incubation region allowing for a longer and more consistent incubation time. A wide serpentine channel was used for droplet incubation. Different lengths of incubation channel were used with incubation times typically of 15-20 minutes. The incubation time allows for a decrease in pH of droplets containing cells due to secretion of lactate. At the end of the incubator, the channel narrowed before entering the sorting region of the chip. The Oil and Droplet Outlet and QX100 Inlet served two functions. The first was to control the number and rate of droplets entering the sorting region. This is necessary because if too many droplets enter the sorting region, inter-droplet interactions will dominate over the differences of droplet interfacial tension. The second purpose is to replace the oil and surfactant from picosurf-1 to QX100 for reasons described in detail below. A negative flow is applied at the Oil and Droplet Outlet, removing a sizable fraction of both droplets and the oil. This is followed downstream by a QX100 Inlet that effectively dilutes the picosurf-1 at the expense of QX100.

The oil with surfactant is changed from picosurf-1 to QX100 right before the droplets enter the cell sorting region containing the rail. The change of surfactant was found to be necessary for several reasons. First, QX100 was found to impede lactate production in cells, thus it was necessary to introduce QX100 only after incubation to allow a pH difference to develop between droplets containing cells and empty droplets. Ionic surfactants, as QX100 is believed to be, have poor biocompatibility.[39] While the addition of pluronic to the formulation improved biocompatibility and droplet stability,[33] best results were obtained by limiting the cell exposure to QX100. Lastly, the pH dependent change in interfacial tension decreased over time after the formation of

droplets and it proved difficult to sort droplets after several minutes of droplets exposure to QX100. The exact source of this time dependent change in interfacial tension is unknown but may be due to the either the transport of surfactants to the interface or the reorganization of surfactants at the droplet interface.

SORTING DROPLETS OF DIFFERENT pH

The principle and function of the sorter is demonstrated for droplets of different pH in Figure 2 and supplemental video S1. Physical dimensions of the sorter region of the chip are provided in Figure S3. The sorting uses the general techniques of "Rails and Anchors".[40,41] Without additional forces, droplets take the shape that minimizes their surface area, a sphere. In this device, the channel height (25 μm) is smaller than the droplet diameter of typically 50-80 μm. The droplets are therefore pancake shaped, squeezed by the top and bottom surfaces of the channel (inset Fig 2). A microfabricated trench, the rail, has an increased height (40 μm) relative to the rest of the channel. The droplets change shape after entering the rail, reducing their overall surface area (green droplet at bottom of rail). The rail retains the droplet as the droplets are more confined upon exiting the rail. The retaining force of the rail is proportional to the interfacial tension.

Droplets of low interfacial tension (red droplets) enter the rail but are pushed off the rail immediately by the oil flow. Droplets of higher interfacial tension (green droplets) remain on the rail and are pushed up along the rail that is oriented at 45° with respect to the flow direction. The rail is tapered. As the droplet follows the rail upwards, droplets are only partially in the rail as the rail width becomes narrower than the droplet

diameter (top two green droplets on rail). The droplet surface area increases as the droplet follows the rail upwards. When the force of the entrainment oil flow overcomes the retaining force the droplet is pushed off the rail. The droplet exits the rail at a different lateral position then a droplet of lower interfacial tension. This principal allows the sorting of droplets with different interfacial tensions and also pH using the dependency presented in Fig 1a.

Figure 2 and video S1 shows the sorting of two populations of droplets of different pH. The droplets enter the sorting region near the bottom of the channel and encounter the lower and wider portion of the sorting rail. Droplet of high pH (white droplet), or low interfacial tension, are pushed off the rail towards the Un-Selected Droplet Outlet. The low interfacial tension of white droplets is also noticeable by the large distortion in droplet shape as it exits the rail. Droplets of low pH (clear droplets) and high interfacial tension follow the rail laterally upwards. They leave the rail as it narrows to a point and flow to the Target Droplet Outlet. The two droplet outlets enable the collection of the two populations of droplets and cells off-chip.

As the sorting is based on a physical principle, it is reproducible and robust. Sorting errors are rare but occur due to droplet interactions as droplet bunching can occasionally push off a droplet from the rail earlier than expected for a given droplet pH. These can be minimized by adjusting flow rates to allow sufficient spacing between droplets.

Figure S4 characterizes the displacement on the sorting rail as a function of pH, droplet diameter and oil entrainment flow. For high pH droplets, droplets leave the rail in the lower portion of the rail while low pH droplets follow the rail (Fig. S4a). The change

in displacement on the rail occurs over a small pH range. For the droplet size (70-75μm) and entrainment flow (45 μL/min) presented, a sudden change in droplet position occurs between pH 7.16 and 6.89. More generally, we have found that the device can effectively sort droplets with ΔpH of 0.4 at a rate of about 30 Hz. The sorting of droplets is quite sensitive to size (Fig S4b), with droplets of diameter 65 μm or smaller following the rail to the top while 80 μm or greater do not climb the rail (droplets at pH 7.11 and entrainment flow 40 μL/min). This shows that the device can be used as an effective method to sort droplets based on size. The Oil Entrainment Inlet (Fig 1b) allows a control of the entrainment flow in the sorting region. The flow can be adjusted to sort within a desired droplet size and pH range. As shown in Fig S4c, as the entrainment flow increases, droplets initially follow the rail at lower flows but are pushed off at higher flows. In the data presented (droplets at pH 7.11 and diameter 75-80 μm), droplets follow the rail at 30 μL/min. At 35 μL/min, approximately 50% of droplets climb the rail. At higher flow rates, droplets are pushed off the rail. A small number of droplets still climb the rail even at high flow rates, possibly due to slightly smaller size.

CHANGE of pH of DROPLETS

SIFT's ability to sort droplets relies on the development of a distinct pH difference after incubation between droplets containing cells and empty droplets. U87 glioblastoma cells have been shown to have high single-cell lactate secretion rates even under ambient oxygen conditions, and were thus chosen for our study.[42] To determine droplet pH after incubation, pyranine, a fluorescence ratiometric pH sensor was used.[43] Pyranine has a pH sensitive absorption spectra allowing a pH determination from the

ratio of fluorescence from excitations in the violet (395 nm) and blue (440 nm) using a calibration curve (supplemental figure S5). As pyranine is membrane impermeable, it provides a pH readout of the droplet and not of the cell. The fast movement of droplets did not allow for accurate pH determinations while sorting.

Immediately after droplet encapsulation, all droplets show the same fluorescence corresponding to the initial cell solution pH of 7.5. However over time, droplets containing cells show a marked change in fluorescence due to acidification from the secretion of lactate. Figure 3a and 3b shows the typical fluorescence images after 15 minutes of incubation with violet and blue excitation, respectively. Images were taken at the end of the incubator just prior to the sorting rail. A few cells are circled in green, visible as bright spots in Figure 3a (due to cell auto-fluorescence) and dark spots in Figure 3b. Concurrent with a drop in pH, droplets containing cells appear brighter with violet excitation and dimmer with blue excitation as compared to empty droplets. However it is worth noting that droplets containing a cell show a marked variance in fluorescence intensity, reflecting the varied glycolysis rates in single cells.

From the fluorescence, the pH of empty droplets was determined to be 7.51 ± 0.03 (*N=30)* (average ± standard deviation), unchanged from the initial buffer solution pH. Droplets containing one and two cells were determined to be at pH 7.17 ± 0.10 (*N=29)* and 6.84 ± 0.23 (*N=6)*. The variance in pH of droplet containing cells is expected from the cell-to-cell variability in lactate secretion rates as observed in a previous study.[44] Droplets containing cells form a distinct population from empty droplets with a pH of 0.34 units lower on average. This difference in pH leads to concurrent change in interfacial tension that is used to select live cells in the device.

SINGLE-CELL ENCAPSULATION

Most droplet microfluidic applications that measure single cells require single cell occupancy in each droplet. The cell occupancy is determined by the concentration of cells in the aqueous phase and Poisson statistics. This leads to the situation where either low concentrations of cells are used (< 0.1 cells per droplet volume) that leaves most droplets empty for analysis but avoids double cell occupancy. Otherwise, higher concentrations are used (1 cell per droplet volume) but multiple cell occupancies must be tolerated and at best 37% of droplets will contain a single cell.[39] For this reason, several techniques, both active and passive, have been developed to ensure one cell per droplet.[45,46] SIFT presents a passive method based on single cell glycolytic activity to ensure single occupancy.

Figure 4 and supplemental video S2 shows the sorting of droplets containing cells from empty droplets. To facilitate visualization, cells were tagged with a fluorescence cell marker prior to analysis. Droplets enter at the bottom of the image. Cell density was kept low (5.6% of droplets contain cells) so that most droplets entering the sorter were empty. Droplets that do not contain cells are only slightly deflected laterally by the rail and exit the rail near the bottom. Droplets containing cells ride the rail upwards and exit the rail near the top of the image. The technique is effective at isolating droplets containing cells while excluding all empty droplets. Of the droplets entering the sorter (N=1006), only droplets containing cells were selected (N=41). Some selected droplets are expected to also contain two or more cells. Multiple cell occupancy can be minimized by keeping overall cell density low. Not all droplets containing cells were selected as 25

% of the total cells analyzed were not selected (*N*= 14). Many of these droplets partially climbed the rail before being bumped off the rail by other droplets. These unselected cells could also represent cells with low levels of lactate secretion.

LIVE vs. DEAD SORTING

Live vs. dead cell detection and sorting is routinely used for pharmacology and toxicology.[47] Glycolysis is a clear indication of cell viability and used to detect and sort live cells. A subpopulation of dead cells from treatment with paraformaldehyde was mixed with untreated cells. CellTracker™ viability probe was used to distinguish the live and dead cell populations and evaluate the sorting accuracy. Similar incubation conditions were used as the single-cell encapsulation experiment above. After incubation, droplets containing dead cells remain at the initial buffer pH while droplets containing cells have a lower pH.

Figure 5 and supplemental video S3 shows the sorting of live and dead cells with live cells fluorescent within the central portion of the image. In this application, a sorting rail with a horizontal section was used to lead droplets to the angled rail (dimensions provided in Fig. S3b). Droplets containing live cells follow the rail upwards while empty droplets and droplets containing dead cells are only slightly deflected by the rail.

The device was shown to select exclusively droplets containing live cells while excluding droplets containing dead cells or no cells. Of the total droplets analyzed (*N*= 1421), the percentage of droplets containing live (*N*=75) and dead cells (*N*=51) corresponded to 5.3% and 3.6%, respectively. Only droplets containing live cells (*N*=42) were selected that include both single cell occupancy (*N*=23) and multiple cell occupancy

(*N*=19). The higher proportion of multiple cell occupancy than expected was due to a small degree of cell clumping. Some dead cells are likely selected in the droplets with multiple cell occupancy however the resolution of the videos did not allow accurate quantification. The device collected only a portion of the live cells as 44 % of droplets containing live cells were not selected (*N*=33) by the device.

Conclusions

We have shown that under specific surfactant conditions a difference in pH can change the interfacial tension of aqueous droplets. Leveraging this relationship, we have developed SIFT, a robust, label-free microfluidic method capable of selecting droplets based on pH. SIFT was applied to enable single cell encapsulation and selection of live mammalian cancer cells. The technique utilizes a novel and robust droplet selection criterion, glycolytic activity, to isolate live cells.

This passive technique is based on a physical change in droplet properties, and is thus predictable, and relatively error-free. Buffer capacity can be used to tune the sensitivity of the device to the acidification rate. Due to the lack of active components, SIFT is also an inexpensive solution. This not only simplifies device design but enables sorting elements to be easily replicated and used in parallel to achieve very high throughput.

As the first iteration of this device, there is potential for improvements in both sensitivity and throughput via optimization of channel features and flow conditions. The current device has the sensitivity to sort individual cells with sorting rates of approximately 30 droplets per second. Sensitivity to small pH changes is important to

sort cell types with low glycolytic rates. It was found that droplets with a difference as little as 0.2 pH units will exit the rail at different positions. We observed that exposure of cells to QX100 during the droplet sorting step can influence cell viability after sorting. This may not be an issue for certain downstream analysis such as sequencing but would be undesirable for applications that rely on a large recovery of live cells. The viability may be improved by optimizing formulation while at the same time minimizing cellular exposure to QX100 oil solution.

We chose here long incubation times to create a binary population of droplets for separating live cells from empty droplets and dead cells. However, an adjustment of incubation times or buffer conditions can be used to gather a cell subpopulation of high lactate producers. This is of interest in oncology as high levels of lactate release have been associated with metastasis, tumor recurrence and poor outcomes.[48–51] In this light, single cells that exhibit high lactate secretion rates are expected to be more malignant and therefore specific targets for cancer therapy.[52]

This device was used to sort cultured cancer cells that have elevated lactate secretion rates that can be 30 fold higher than normal cells.[53,54] However, the technique can be extended for sorting a broad range of cell types by stimulating anaerobic glycolysis by performing the incubation step in low oxygen conditions. As cellular glycolysis is ubiquitous, the sorting strategy technology described here can have an impact in sorting or selection across diverse cell types for applications in many fields including bioenergy, biotechnology and medicine.

Supporting Information Available: This material is available free of charge via the Internet at http://pubs.acs.org.

Acknowledgements

We acknowledge helpful discussions with David Hess, Angel Islas and On Shun Pak at Santa Clara University. We thank Bill Lu (Department of Bioengineering, Santa Clara University) for providing cells. SB and BL acknowledge generous funding from ALZA through the ALZA Corporation Science Scholar program. We would also like to thank International Electronic Components Inc. for their generous donation of dry photoresist. Paul Abbyad is supported for this project by a National Science Foundation Career Award, Grant Number 1751861 and the National Institutes of Health under grant 1R15GM129674-01.

References

(1) Gregory, C. D.; Pound, J. D.; Devitt, A.; Wilson-Jones, M.; Ray, P.; Murray, R. J. *MAbs* **2014**, *1*, 370–376.

(2) Yang, H.; Acker, J. P.; Cabuhat, M.; Letcher, B.; Larratt, L.; McGann, L. E. *Bone Marrow Transplant.* **2005**, *35*, 881–887.

(3) Wang, B. L.; Ghaderi, A.; Zhou, H.; Agresti, J.; Weitz, D. A.; Fink, G. R.; Stephanopoulos, G. *Nat Biotech* **2014**, *32*, 473–478.

(4) Agresti, J. J.; Antipov, E.; Abate, A. R.; Ahn, K.; Rowat, A. C.; Baret, J.-C.; Marquez, M.; Klibanov, A. M.; Griffiths, A. D.; Weitz, D. A. *Proc. Natl. Acad. Sci.* **2010**, *107*, 4004–4009.

(5) Baret, J.-C.; Miller, O. J.; Taly, V.; Ryckelynck, M.; El-Harrak, A.; Frenz, L.; Rick, C.; Samuels, M. L.; Hutchison, J. B.; Agresti, J. J.; Link, D. R.; Weitz, D. A.; Griffiths, A. D. *Lab Chip* **2009**, *9*, 1850–1858.

(6) Sciambi, A.; Abate, A. R. *Lab Chip* **2015**, *15*, 47–51.

(7) Gee, A. P.; Durett, A. G. In *Cytotherapy*; 2002; Vol. 4, pp 91–92.

(8) Yang, A. H. J.; Soh, H. T. *Anal. Chem.* **2012**, *84*, 10756–10762.

(9) Zalis, M. C.; Reyes, J. F.; Augustsson, P.; Holmqvist, S.; Roybon, L.; Laurell, T.; Deierborg, T. *Integr. Biol.* **2016**, *8*, 332–340.

(10) Kwon, T.; Yao, R.; Hamel, J. F. P.; Han, J. *Lab Chip* **2018**, *18*, 2826–2837.

(11) Hur, S. C.; Henderson-MacLennan, N. K.; McCabe, E. R. B.; Di Carlo, D. *Lab Chip* **2011**, *11*, 912–920.

(12) Tottori, N.; Nisisako, T.; Park, J.; Yanagida, Y.; Hatsuzawa, T. *Biomicrofluidics* **2016**, *10*.

(13) Shafiee, H.; Sano, M. B.; Henslee, E. A.; Caldwell, J. L.; Davalos, R. V. *Lab Chip* **2010**, *10*, 438–445.

(14) Patel, S.; Showers, D.; Vedantam, P.; Tzeng, T. R.; Qian, S.; Xuan, X. *Biomicrofluidics* **2012**, *6*, 1–12.

(15) Gossett, D. R.; Weaver, W. M.; MacH, A. J.; Hur, S. C.; Tse, H. T. K.; Lee, W.; Amini, H.; Di Carlo, D. *Anal. Bioanal. Chem.* **2010**, *397*, 3249–3267.

(16) Hessler, J. A.; Budor, A.; Putchakayala, K.; Mecke, A.; Rieger, D.; Holl, M. M. B.; Orr, B. G.; Bielinska, A.; Beals, J.; Baker, J. *Langmuir* **2005**, *21*, 9280–9286.

(17) Danø, S.; Sørensen, P. G.; Hynne, F. *Nature* **1999**, *402*, 320–322.

(18) Cangelosi, G. A.; Meschke, J. S. *Appl. Environ. Microbiol.* **2014**, *80*, 5884–5891.

(19) DeBerardinis, R. J.; Thompson, C. B. *Cell* **2012**, *148*, 1132–1144.

(20) Webb, B. A.; Chimenti, M.; Jacobson, M. P.; Barber, D. L. *Nat. Rev. Cancer* **2011**, *11*, 671–677.

(21) Mookerjee, S. A.; Goncalves, R. L. S.; Gerencser, A. A.; Nicholls, D. G.; Brand,

M. D. *Biochim. Biophys. Acta - Bioenerg.* **2015**, *1847*, 171–181.

(22) Wu, M.; Neilson, A.; Swift, A. L.; Moran, R.; Tamagnine, J.; Parslow, D.; Armistead, S.; Lemire, K.; Orrell, J.; Teich, J.; Chomicz, S.; Ferrick, D. A. *Am. J. Physiol. Cell Physiol.* **2007**, *292*, C125-36.

(23) Warburg, O. H. *Naturwissenschaften* **1924**, *12*, 1131–1137.

(24) Warburg, O. *Science* **1956**, *123*, 309–314.

(25) Del Ben, F.; Turetta, M.; Celetti, G.; Piruska, A.; Bulfoni, M.; Cesselli, D.; Huck, W. T. S.; Scoles, G. *Angew. Chemie - Int. Ed.* **2016**, *55*, 8581–8584.

(26) Kurup, G. K.; Basu, A. S. *Micro Total Anal. Syst. 2012* **2012**, 76–78.

(27) Kurup, G. K.; Basu, A. S. *Micro Total Anal. Syst. 2013* **2013**, 1344–1346.

(28) Collins, D. J.; Neild, A.; DeMello, A.; Liu, A. Q.; Ai, Y. *Lab Chip* **2015**, *15*, 3439–3459.

(29) Stephan, K.; Pittet, P.; Renaud, L.; Kleimann, P.; Morin, P.; Ouaini, N.; Ferrigno, R. *J. Micromech. Microeng.* **2007**, *17*, N69.

(30) Abramoff, M. D.; Magalhaes, P. J.; Ram, S. J. *Biophotonics Int.* **2004**, *11*, 36–43.

(31) Thorsen, T.; Roberts, R. W.; Arnold, F. H.; Quake, S. R. *Phys. Rev. Lett.* **2001**, *86*, 4163–4166.

(32) Pekin, D.; Skhiri, Y.; Baret, J.-C.; Le Corre, D.; Mazutis, L.; Salem, C. Ben; Millot, F.; El Harrak, A.; Hutchison, J. B.; Larson, J. W.; Link, D. R.; Laurent-Puig, P.; Griffiths, A. D.; Taly, V. *Lab Chip* **2011**, *11*, 2156–2166.

(33) Brouzes, E.; Medkova, M.; Savenelli, N.; Marran, D.; Twardowski, M.; Hutchison, J. B.; Rothberg, J. M.; Link, D. R.; Perrimon, N.; Samuels, M. L. *Proc. Natl. Acad. Sci.* **2009**, *106*, 14195–14200.

(34) Debs, B. El; Utharala, R.; Balyasnikova, I. V; Griffiths, A. D.; Merten, C. A. *Proc. Natl. Acad. Sci.* **2012**, *190*, 11570–11575.

(35) Huebner, A.; Bratton, D.; Whyte, G.; Yang, M.; Demello, A. J.; Abell, C.; Hollfelder, F. *Lab Chip* **2009**, *9*, 692–698.

(36) Theberge, A. B.; Whyte, G.; Frenzel, M.; Fidalgo, L. M.; Wootton, R. C. R.; Huck, W. T. S. *Chem. Commun.* **2009**, *2009*, 6225–6227.

(37) Baret, J. C.; Kleinschmidt, F.; El Harrak, A.; Griffiths, A. D. *Langmuir* **2009**, *25*, 6088–6093.

(38) Frenz, L.; Blank, K.; Brouzes, E.; Griffiths, A. D. *Lab Chip* **2009**, *9*, 1344–1348.

(39) Clausell-Tormos, J.; Lieber, D.; Baret, J. C.; El-Harrak, A.; Miller, O. J.; Frenz, L.; Blouwolff, J.; Humphry, K. J.; Köster, S.; Duan, H.; Holze, C.; Weitz, D. A.; Griffiths, A. D.; Merten, C. A. *Chem. Biol.* **2008**, *15*, 427–437.

(40) Abbyad, P.; Dangla, R.; Alexandrou, A.; Baroud, C. N. *Lab Chip* **2011**, *11*, 813–821.

(41) Fradet, E.; McDougall, C.; Abbyad, P.; Dangla, R.; McGloin, D.; Baroud, C. N. *Lab Chip* **2011**, *11*, 4228–4234.

(42) Mongersun, A.; Smeenk, I.; Pratx, G.; Asuri, P.; Abbyad, P. *Anal. Chem.* **2016**, *88*, 3257–3263.

(43) Bai, Z.; Chen, R.; Si, P.; Huang, Y.; Sun, H.; Kim, D. *Appl. Mater. Interfaces* **2013**, 2–6.

(44) Mongersun, A.; Smeenk, I.; Pratx, G.; Asuri, P.; Abbyad, P. *Anal. Chem.* **2016**, *88*, 3257–3263.

(45) Chabert, M.; Viovy, J.-L. L. *Proc. Natl. Acad. Sci.* **2008**, *105*, 3191.

(46) Edd, J. F.; Di Carlo, D.; Humphry, K. J.; Köster, S.; Irimia, D.; Weitz, D. A.; Toner, M. *Lab Chip* **2008**, *8*, 1262–1264.

(47) Wlodkowic, D.; Faley, S.; Darzynkiewicz, Z.; Cooper, J. M. *Methods Mol. Biol.* **2011**, *731*, 285–291.

(48) Walenta, S.; Mueller-Klieser, W. F. *Semin. Radiat. Oncol.* **2004**, *14*, 267–274.

(49) Doherty, J.; Cleveland, J. *J. Clin. Invest.* **2013**, *123*, 3685–3692.

(50) Martinez-Outschoorn, U. E.; Prisco, M.; Ertel, A.; Tsirigos, A.; Lin, Z.; Pavlides, S.; Wang, C.; Flomenberg, N.; Knudsen, E. S.; Howell, A.; Pestell, R. G.; Sotgia, F.; Lisanti, M. P. *Cell Cycle* **2011**, *10*, 1271–1286.

(51) Cairns, R. A.; Harris, I. S.; Mak, T. W. *Nat. Rev. Cancer* **2011**, *11*, 85–95.

(52) Hirschhaeuser, F.; Sattler, U. G. A.; Mueller-Klieser, W. *Cancer Res.* **2011**, *71*, 6921–6925.

(53) Holm, E.; Staedt, U.; Schlickeiser, G.; Leweling, H.; Tokus, M.; Hagmüller, E.; Gtinther, H. J.; Kollmar, H. B. *Cancer Res.* **1995**, *55*, 1373–1378.

(54) DeBerardinis, R. J.; Mancuso, A.; Daikhin, E.; Nissim, I.; Yudkoff, M.; Wehrli, S.; Thompson, C. B. *Proc. Natl. Acad. Sci. U. S. A.* **2007**, *104*, 19345–19350.

Figures

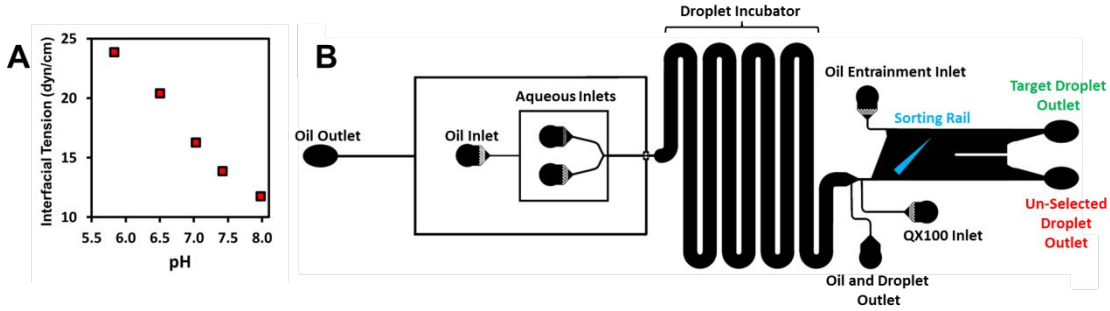

Figure 1. a) Interfacial Tension vs. pH for droplets containing media (DMEM) in QX100 diluted 100 fold with Novec 7500 at room temperature. **b)** Schematic of droplet sorting device channel geometry.

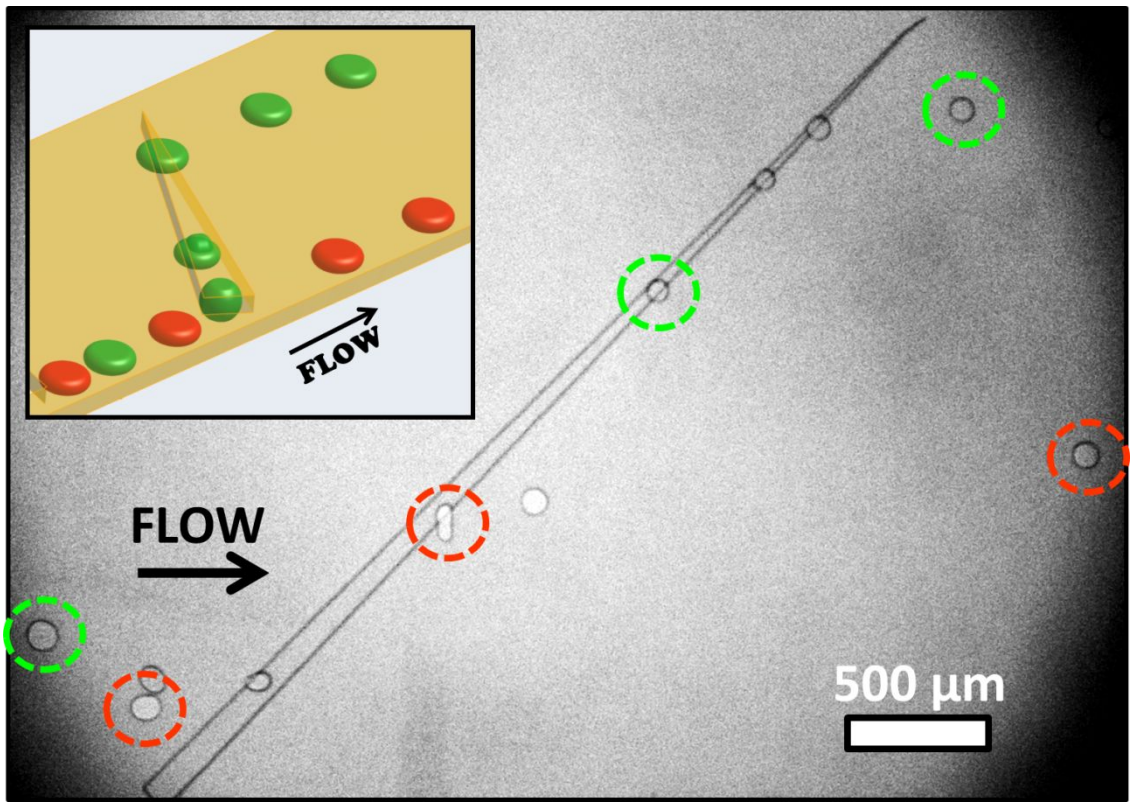

Figure 2. Selection of droplets of different pH using SIFT. White droplets (pH: 7.55) of lower interfacial tension deflect off the rail in the lower portion of rail. Clear droplets (pH: 6.96) of higher interfacial tension climb the rail upwards. Several droplets are circled in red (pH: 7.55) and green (pH: 6.96) to emphasize the droplet path. A low concentration of fluorescein was added to droplets of pH 7.55 to identify the two droplet populations. **Inset:** Schematic of droplet selection rail of high (green) and low (red) interfacial tension droplets. Shape change in rail is exaggerated for illustrative purposes.

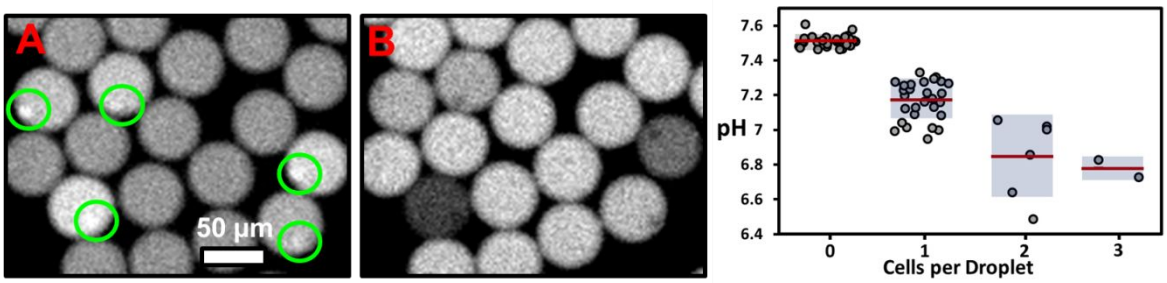

Figure 3. **a)** Fluorescent image with violet excitation (395 nm) after droplet incubation. Droplets contain pyranine, a ratiometric pH probe. Individual cells are circled in green. Droplets containing cells appear brighter than empty droplets. **b)** Fluorescent image with blue excitation (440 nm). Droplets containing cells appear dimmer than empty droplets. **c)** pH of droplets containing zero to three U87 cells as determined from fluorescence intensity ratio. Average value is indicated by a red line and standard deviation by a grey bar.

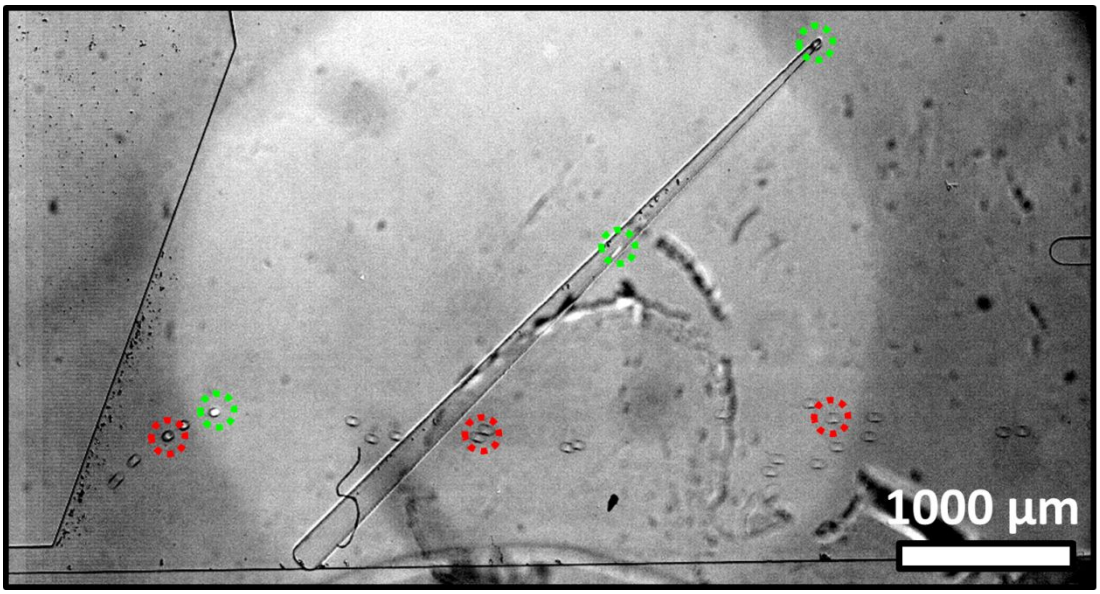

Figure 4. Selection of droplets containing single cells by SIFT. Droplets enter the image from bottom left. Droplets that do not contain cells (a few circled in red) are only slightly deflected by the sorting rail and flow off the rail near the bottom. Droplets containing cells (circled in green), ride the rail laterally up and exit the rail near the top. The cells were stained with fluorescent dye, Calcein-AM, for better visibility. Fluorescent excitation is localized in a hexagonal central region of the imaging field.

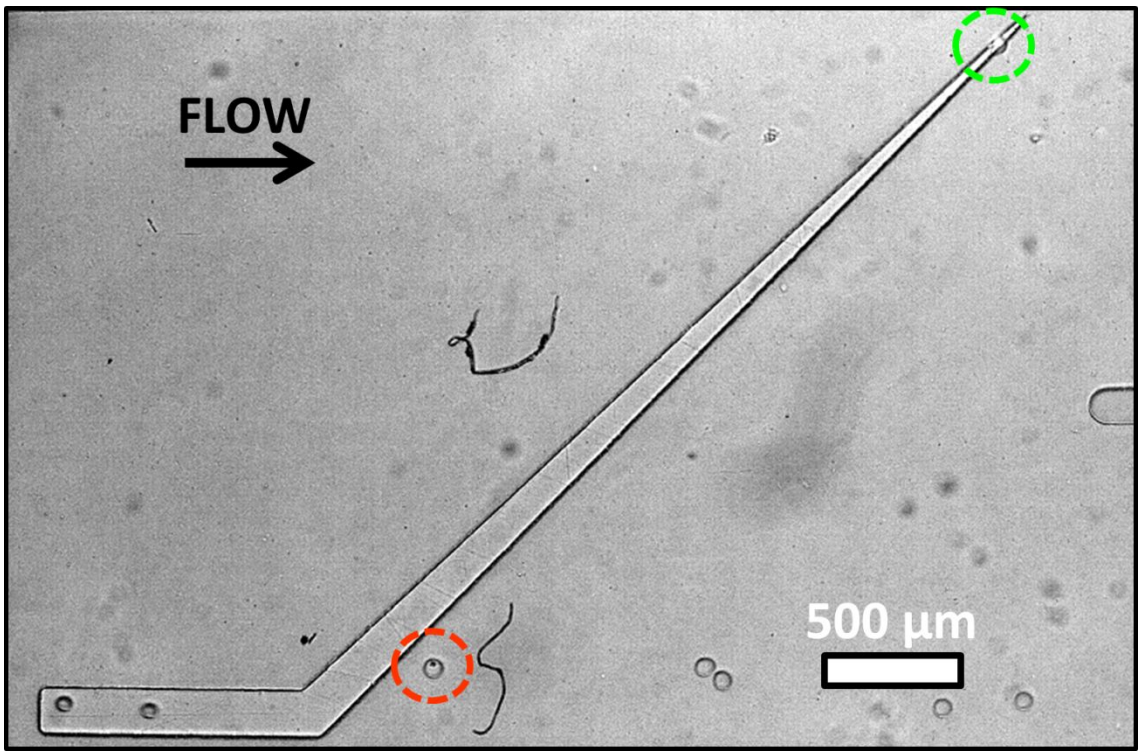

Figure 5. Live vs. dead selection. Droplets enter the image from bottom left. Droplets that do not contain cells or contain dead cells (one circled in red) are only slightly deflected by the sorting rail and flow off the rail near the bottom. Droplets containing a single cell (circled in green), rides the rail laterally up and leaves the rail near the top. Live cells were stained with fluorescent viability dye, Calcein-AM.

A new label-free and passive microfluidic technique to select cells based on single-cell glycolytic activity. The method has broad applicability and we demonstrate here single-cell droplet encapsulation and selection of live cells.

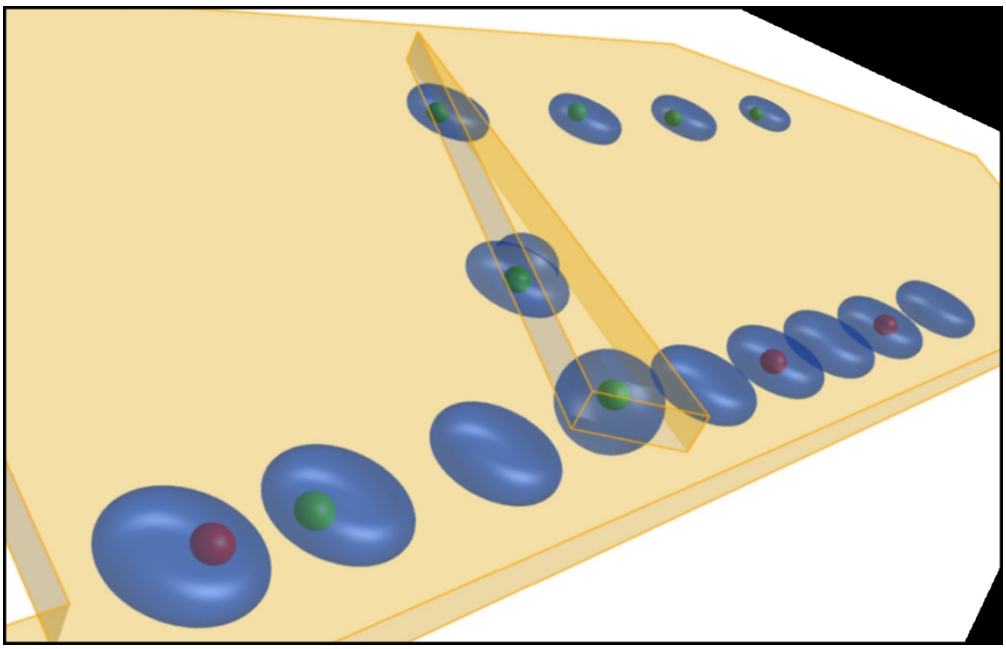

211x135mm (150 x 150 DPI)